Static and high frequency magnetic and dielectric properties of ferrite-ferroelectric composite materials

Sangita S. Kalarickal,[a] David Ménard,[b] Jaydip Das, and Carl E. Patton
Department of Physics, Colorado State University, Fort Collins, Colorado 80523

Xubai Zhang, Louise C. Sengupta, and Somnath Sengupta
Paratek Microwave Inc., Columbia, Maryland 21045

(Received 8 December 2005; accepted 25 July 2006; published online 20 October 2006)

A series of sintered composite materials was fabricated from Parascan™ barium strontium titanate (BSTO) and Trans-Tech nickel zinc ferrite powders. The ferrite loading was varied from zero (BSTO only) to 100 wt % (ferrite only). X-ray diffraction data show the presence of a third, nonmagnetic phase that sets the ferrite loading at values somewhat lower than the as prepared wt % amounts. The average magnetization is found to scale linearly with the loading. The initial susceptibility, saturation field, and coercive force as obtained from hysteresis loop data show trends consistent with these data. Ferromagnetic resonance linewidth and effective linewidth measurements at 10 GHz show reasonable values for the 100 wt % samples, but any amount of BSTO causes a severe degradation in both loss parameters. Similarly, it is found that any amount of ferrite causes a rapid drop in the relative dielectric constant that is consistent with standard mixing models. Loss tangent measurements gave modest values in the 0.001–0.005 range at 1 MHz and much larger values in the 0.02–0.03 range at 10 GHz. © *2006 American Institute of Physics*. [DOI: 10.1063/1.2357990]

I. INTRODUCTION

Ferrites and ferroelectric materials are used in a large family of microwave and millimeter wave devices. Ferrite devices typically have high figures of merit, large bandwidths, low insertion loss, and frequency agility.[1] Current ferrite components, however, present two critical problems for advanced system applications: large size and high cost. Ferroelectric components, on the other hand, provide solutions both in size and cost.[2,3] Size reduction arises from the large relative dielectric constants. These components are also tunable with the application of a modest voltage. Since the tunability is not as good as for ferrites, the voltage tunability and the low cost are advantageous for many applications.

It is likely that ferrite-ferroelectric composites could be used to produce small, low cost, and highly tunable elements for microwave applications. Because of the wide variety of possible applications, there has been considerable interest in composite materials.[4–14] Previous works on multifunctional ferrite-ferroelectric composite materials have emphasized static magnetization properties[4,14] and complex permeability and permittivity.[15] The objective of this work was to prepare a series of ferrite-ferroelectric composite materials with a systematic variation in the ferrite loading and to examine the static and high frequency magnetic properties and dielectric properties of these materials. The magnetic component was a standard commercial nickel zinc spinel ferrite (NZF) from Trans-Tech, TT2-111. The ferroelectric component was specially prepared barium strontium titanate (BSTO).

X-ray diffraction (XRD) data indicate that the processing produced a titanium oxide phase in addition to the NZF and BSTO phases. Electrical permittivity measurements indicate changes that scale with loading in a manner that is consistent with electromagnetic mixing models. Static and dynamic magnetic property measurements generally scale with the amount of the ferrite component. The composites generally show high loss, both electrical and magnetic. These results indicate that further work is needed to produce composites that (1) retain the useful low loss properties of the separate phases and (2) yield the additional multifunctionality needed for tunable microwave devices.

The paper is organized as follows. Section II describes the materials preparation and the XRD results. Section III presents room temperature magnetization versus field data for all of the composites and considers these data in terms of a simple model of noninteracting magnetic particles in a nonmagnetic host. Section IV presents ferromagnetic resonance (FMR) results. Section V extends the high frequency analysis to include the microwave response at magnetic fields well above the FMR resonance field. This response is used to determine the high field effective linewidth for the different loadings. Section VI gives basic data on the dielectric properties of the composites. Section VII presents the summary and conclusions.

II. MATERIALS PREPARATION AND X-RAY CHARACTERIZATION

The composite materials consisted of thick disks of Parascan™ tunable dielectric materials, nominally ferroelectric BSTO, with different loadings of the NiZn ferrite. Different nominal weight percentages of the TT2-111 NiZn ferrite powder (0.3, 1, 5, 10, 25, and 50 wt %) were mixed with

[a]Present address: Institute für Experimentalphysik, Freie Universität Berlin, Arnimallee 14, 14197 Berlin, Germany; electronic mail: sangita@lamar.colostate.edu
[b]Present address: Polytechnique Montréal, Québec, Canada.

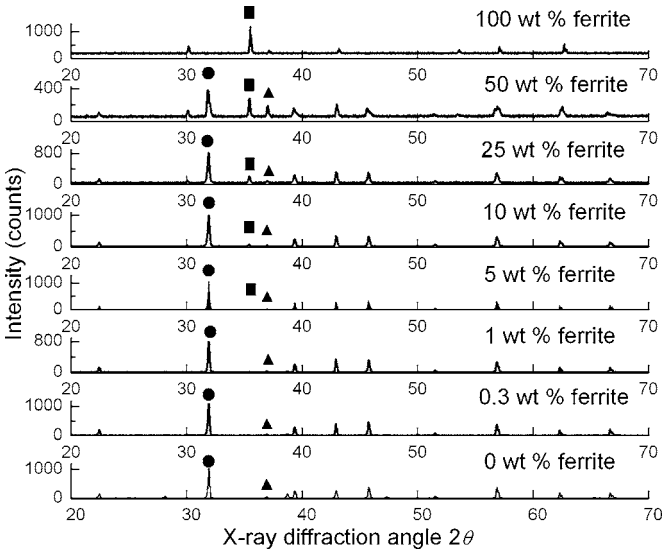

FIG. 1. X-ray diffraction results for all the samples as indicated. The solid circles, squares, and triangles indicate the main peaks for the BSTO, the ferrite phase, and the Ti–O phase.

powders of BSTO materials. In addition, pure TT2-111 powders were independently processed and sintered to produce a fully loaded ferrite reference material. All mixtures were alumina ball milled for 24 h in ethanol. The slurries were then dried and sieved. For each loading, a set of samples was pressed into 1 in. diameter disks and sintered at various temperatures of 1200–1450 °C. A sintering temperature of 760 °C was determined to yield the highest overall density for the pure BSTO material. Disk densities were then measured. Optimum density samples were used for all of the measurements reported below. Sample densities, as measured on the starting cubes for the sphere samples used for the magnetic measurements (see below), ranged from 4.20 to 5.25 g/cm^3. There was no apparent correlation between loading and density.

A full x-ray diffraction analysis was done in order to check the phases in the fired materials. The measurements were made with a Bruker AXS system with a copper x-ray source, a scintillation detector, and an angular step size of 0.02°. Figure 1 shows a collage of XRD intensity versus angle of 2θ scans for all the samples. The individual scans are identified by the nominal NZF loading values in wt % for the different samples. In each scan, solid circles and solid squares serve as markers for the main BSTO and NZF diffraction peaks, respectively. The solid triangles mark the peaks that identify the additional Ti–O phase. For the 1 and 0.3 w % samples, there are no resolved NZF peaks.

These XRD data show that the basic mixing of the BSTO and NZF components of the composite takes place as intended. The size of the BSTO peak decreases somewhat as the ferrite loading is increased, and the NZF peaks increase. The integrity of the peaks also indicates that there is no degradation of these primary phases due to the preparation process. The critical result from the XRD data is in the identification of a small titanium oxide component in the final materials. The magnetic data presented below indicate that this phase has no effect other than an overall dilution. Insofar as the focus of this work is on magnetic properties, no work has been done to further identify the chemical makeup or the crystallographic nature of this phase.

The effective loading of the ferrite component of the composite in vol %, taken as L, will play an important role in the data presentation and discussion in subsequent sections. The L values for the different samples were deduced from the relative areas under the main peaks for the three phases identified in Fig. 1. Due to the additional titanium oxide phase, the nominal ferrite loadings of 50, 25, 10, and 5 wt % from the preparation process are converted to L values of 27, 16, 6, and 4 vol %, respectively.

Magnetic and microwave measurements were made on spherical samples with nominal diameters of 2 mm. For these measurements, spheres were fabricated from 3 mm cubes cut from the optimum density fired disks. The densities of the individual cubes and spheres were different from the densities measured on the starting disks, with about the same spread as indicated above. These variations in density may be taken as an indication of inhomogeneous starting disks. Two types of pure ferrite samples were also measured. First, the TT2-111 powders were used to fire disks and then fabricate spheres at 100 vol % ferrite loading based on the same procedures given above. Second, fired TT2-111 blocks from Trans-Tech were used to fabricate sphere samples for base line magnetic and microwave measurements.

All dielectric measurements were made directly on as fired disks. The low frequency dielectric measurements were made on 0.064 cm thick and 2 cm diam disks with screen printed with silver electrodes on both faces. The microwave dielectric measurements were made on discs with a 49.5 mm diameter and a thickness of 0.5 mm with no electrodes.

III. STATIC MAGNETIC PROPERTIES

Static magnetic induction versus field data were obtained by vibrating sample magnetometry at room temperature for applied fields up to 5 kOe. The data below are given in terms of the magnetic induction $4\pi M$. Volumes were calculated from the densities of the fired disks and the masses of the individual samples. Cubes and spheres gave similar results for all the loadings. The specific data below for the materials with partial ferrite loadings were obtained on spheres. Figures 2–4 show data on the saturation induction versus loading, data on magnetization versus field, and various hysteresis loop parameters versus loading, respectively. Considered as a whole, these data show that the static magnetic response is consistent with a model of a composite medium with an unmodified ferrite phase in a nonmagnetic matrix.

Figure 2 shows the data on average saturation induction $\langle 4\pi M\rangle_{sat}$ data versus the ferrite loading L. These measurements were made at an external field of $H=5$ kOe. As the hysteresis data in Fig. 3 will show, a 5 kOe field was sufficient to achieve magnetic saturation. The solid circles show the data for the composite samples. The solid square shows the saturation induction for the TT2-111 reference sphere. The solid line shows the linear response one would expect for an unmodified ferrite phase with a saturation induction value the same as that obtained for $L=100$ vol %.

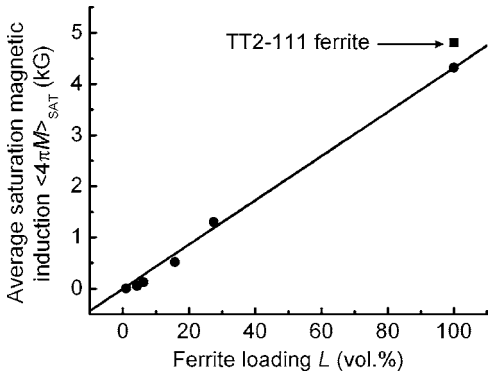

FIG. 2. Average saturation magnetic induction $\langle 4\pi M\rangle_{\text{sat}}$ as a function of ferrite loading L. The data were obtained for an applied magnetic field of 5 kOe. The solid circles show the data for the composites. The solid square shows the value for the commercial TT2-111 ferrite. The solid line shows the linear response expected for an unmodified ferrite phase.

These data serve to make two important points. First, the $\langle 4\pi M\rangle_{\text{sat}}$ value of 4.3 kG at $L=100$ vol % is close to the $\langle 4\pi M\rangle_{\text{sat}}$ value for the standard TT2-111 material. This indicates that the preparation process maintained the basic NZF properties. Second, the data show that the magnetic induction of the sample scales linearly with the ferrite loading. This confirms that the basic ferrite properties for the composite samples were also maintained.

Figure 3 shows full hysteresis loop data on the average magnetic induction $\langle 4\pi M\rangle$ as a function of the applied magnetic field H from −5 to +5 kOe for L values of 4, 6, 16, 27, and 100 vol %. One sees that all of the samples show a clear saturation at some loading dependent $\langle 4\pi M\rangle_{\text{sat}}$ value for fields above 1–2 kOe. As noted above, these $\langle 4\pi M\rangle_{\text{sat}}$ values scale linearly with L.

The Fig. 3 data serve to make two further points. First, from the outward shift in the knee of the hysteresis curves, one can see that the saturation field increases with loading. The 4 and 6 vol % samples have saturation fields well below 500 Oe. For the 100 vol % sample, one has a saturation field $H_{\text{sat}}\approx 1.2-1.4$ kOe. This H_{sat} value for the pure ferrite is very close to one-third of the measured $\langle 4\pi M\rangle_{\text{sat}}$. This means

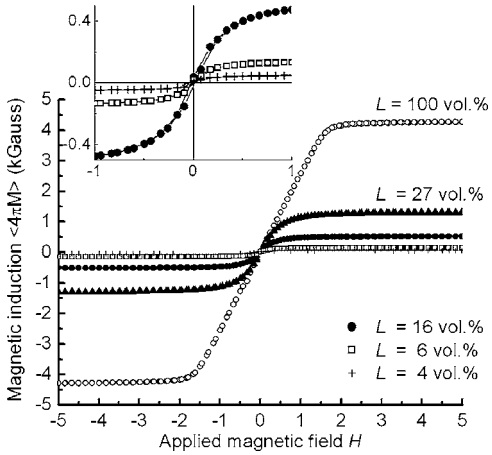

FIG. 3. Average magnetic induction $\langle 4\pi M\rangle$ as a function of the applied magnetic field H for the different ferrite loadings, as indicated. The inset shows an enlarged view for samples with loadings of $L=4$, 6, and 16 vol %.

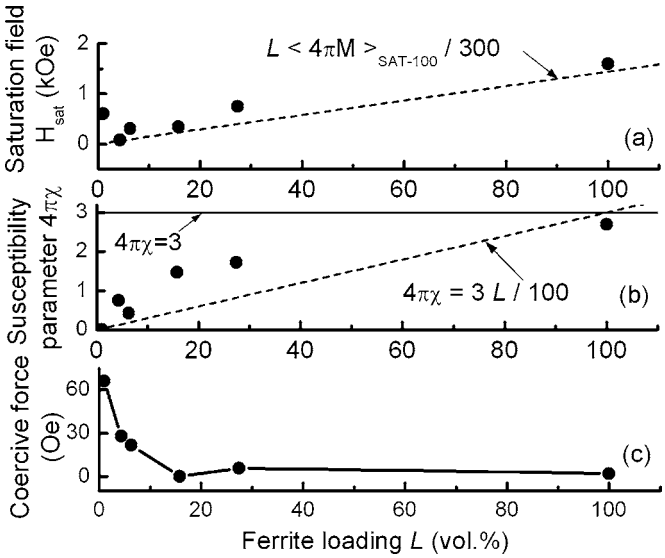

FIG. 4. Saturation field H_{sat}, initial susceptibility $4\pi\chi$, and coercive force H_C as functions of ferrite loading L. The solid circles in (a) show the saturation field data. The dashed line corresponds to $H_{\text{sat}}=L\langle 4\pi M\rangle_{\text{sat-100}}/300$, where $\langle 4\pi M\rangle_{\text{sat-100}}$ is the $\langle 4\pi M\rangle_{\text{sat}}$ value for the 100 vol % sample. The solid circles in (b) show the susceptibility parameter data. The solid line corresponds to $4\pi\chi=3$ and the dashed line corresponds to $4\pi\chi=3L/100$. The solid circles in (c) show the coercive force data.

that the 100 vol % sample behaves as expected from simple demagnetizing field considerations. The lower H_{sat} values for the lower loadings indicate that it is the average mean field saturation induction of the sample as a whole, rather than the saturation induction of the individual NZF grains, that defines the saturation point. If the NZF grains defined the measured H_{sat}, all of the samples would saturate at $H\approx\langle 4\pi M\rangle_{\text{sat-100}}/3$, where "sat-100" refers to the $\langle 4\pi M\rangle_{\text{sat}}$ for $L=100$ vol %. This is discussed in further detail below.

Second, consider the $\langle 4\pi M\rangle$ vs H response in the $H\rightarrow 0$ limit. The slope of this low field response corresponds to $4\pi\chi$, where χ is the initial susceptibility. The data show that as the loading is reduced, the $4\pi\chi$ values also decrease. An effective medium comprised of noninteracting magnetically soft spherical particles would saturate at a field equal to one-third of the saturation induction value. This means that for independent spherical ferrite particles of any kind, the $4\pi\chi$ should depend only on the loading and vary as $3L/100$. Further discussion will follow below

Figure 4 shows results on H_{sat}, $4\pi\chi$, and the coercive force H_C as a function of L, based on the data in Fig. 3. Graph (a) shows H_{sat} values obtained from the extrapolated low field responses shown in Fig. 3 to the $\langle 4\pi M\rangle_{\text{sat}}$ points for each data set. These data are shown by the solid circles. The dashed line corresponds to a linear change in H_{sat} according to $H_{\text{sat}}=L\langle 4\pi M\rangle_{\text{sat-100}}/300$, where $\langle 4\pi M\rangle_{\text{sat-100}}$ is the $\langle 4\pi M\rangle_{\text{sat}}$ value for the 100 vol % sample. Graph (b) shows the $4\pi\chi$ results. The data are shown by the solid circles. The solid line corresponds to the value of $4\pi\chi=3$ expected for a spherical ferrite phase. The dashed line shows the linear $4\pi\chi=3L/100$ response expected for independent ferrite spherical grains. Graph (c) shows the coercive force data. The solid line simply connects the data points.

Apart from the sample with the lowest ferrite loading,

the H_{sat} data in Fig. 4(a) show a nearly linear increase with L and an end point value at $L=100$ vol % that is close to $\langle 4\pi M\rangle_{sat}/3$. The linear response shown by the dashed line is what one would expect from a mean field model, that is, a sample with strongly coupled magnetic particles that acts like a uniformly magnetized material with an $\langle 4\pi M\rangle_{sat}$ equal to $\langle 4\pi M\rangle_{sat\text{-}100}/100$ and $H_{sat}=\langle 4\pi M\rangle_{sat}/3$. The fact that the data lie slightly above the dashed line is an indication that the coupling is not perfect and a mean field model is not strictly applicable. Fully noninteracting particles would give an L-independent H_{sat} equal to $\langle 4\pi M\rangle_{sat\text{-}100}/3$ for all samples.

The $4\pi\chi$ data in Fig. 4(b) show an increase with loading, but the points generally fall well above the linear response line. Interactions between the spherical particles would give an L-independent susceptibility value of 3. Completely independent ferrite inclusions, on the other hand, would give a linear dependence of susceptibility on L. The somewhat larger than linear $4\pi\chi$ values for intermediate L values indicate, therefore, that there may be some level of interaction between the ferrite particles.

The H_C data in Fig. 4(c) show a small coercive force at large loadings and a rapid increase when one drops below $L=16$ vol %. The small values at the large loadings are consistent with the properties of the original TT2-111 material and support the existence of essentially unmodified ferrite grains in the composites down to $L=16$ vol % or so. However, it is not clear why there is such a drastic increase in the coercive force as the loading is reduced below 16 vol %.

IV. FERROMAGNETIC RESONANCE RESPONSE

FMR and high field effective linewidth techniques were used to characterize the microwave losses. This section presents the FMR results. Section V gives the high field effective linewidth results. The FMR profiles were measured by a shorted waveguide reflection technique at an operating frequency f of 9.5 GHz. Measurements were made on nominal 1 mm diameter spheres for the TT2-111 and the 100 vol % materials and nominal 3 mm diameter spheres for the materials with lower loadings. The samples were mounted at the center of the waveguide cross section on a Rexolite® rod and positioned a half wavelength from an adjustable short. The additional loading introduced by the samples at the FMR loss point in field was so small that field modulation and lock-in detection methods were needed to observe the response. The raw data consisted of profiles of the uncalibrated field derivative of the FMR absorption versus field. Absorption profiles of loss versus field were obtained from direct integration of the raw data. These integrated data were then used to determine the resonance field peak position H_{FMR} and the half power linewidth ΔH_{FMR}.

The FMR derivative profiles for the TT2-111 and 100 samples were well resolved and close to the general response expected from dense nickel zinc ferrite materials. The data for the 27 and 16 vol % samples, however, showed that any appreciable drop in the ferrite loading below 100 vol % causes a large degradation in the FMR response. This conclusion is carried over to the extreme for the samples with smaller loadings. These samples showed no recognizable FMR response.

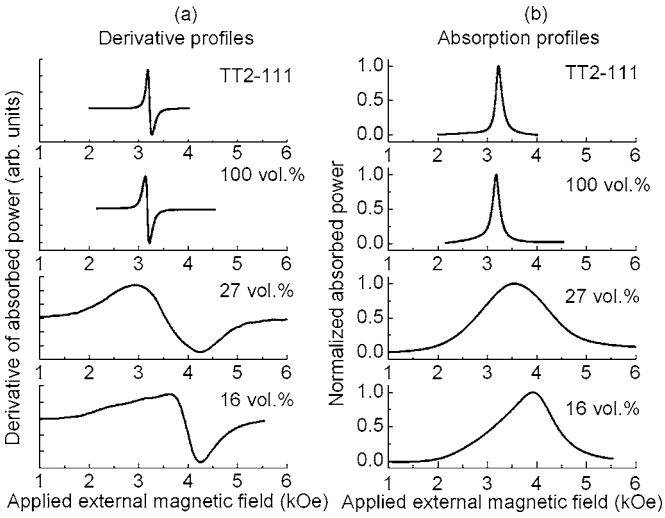

FIG. 5. Ferromagnetic resonance profiles at 9.5 GHz. The (a) graphs show the measured derivative of the absorbed power vs applied magnetic field profiles for the TT2-111, 100, 27, and 16 vol % samples, as indicated. The (b) graphs show the integrated profiles for the derivative profiles in (a).

Figure 5 shows the actual FMR data in two formats. The (a) graphs show the measured derivative of the absorbed power versus applied magnetic field profiles for the TT2-111 and $L=100$, 27, and 16 vol % samples, as indicated. The (b) graphs show the integrated profiles for the derivative profiles in (a). The absorption profiles in (b) have all been scaled to give a peak absorption value of unity. Both the raw data and the integrated profiles show that the FMR lines are narrow and symmetric for the TT2-111 and 100 vol % samples. These line shapes are near Lorentzian. On the other hand, for the 27 and the 16 vol % samples, the absorption profiles are broad and distorted, and nowhere near Lorentzian in shape. One can also see that the peaks for the 27 and the 16 vol % samples are also shifted up in field relative to the FMR positions for the two dense samples.

Table I summarizes the basic FMR parameters obtained from the measurements, namely, the FMR field H_{FMR}, the effective gyromagnetic ratio γ_{eff} expressed in frequency units as $|\gamma_{eff}|/2\pi$, the FMR half power linewidth ΔH_{FMR}, and the high field effective linewidth ΔH_{eff}. The samples are listed according to the vol % loading L values from the XRD data. The FMR field is taken at the peak loss point in the (b)

TABLE I. Summary of 9.5 GHz ferromagnetic resonance (FMR) and effective linewidth measurement results.

Vol % ferrite loading L	FMR field H_{FMR} (Oe)	Effective gyromagnetic ratio $\lvert\gamma_{eff}\rvert/2\pi$	FMR linewidth ΔH_{FMR} (Oe)	High field effective linewidth ΔH_{eff} (Oe)
100 (TT2-111)	3223	2.95	157	6
100	3175	2.99	168	8
27	3549	2.68	1596	97
16	3924	2.42	1260	480
6	⋯	⋯	⋯	367

graphs in Fig. 5. For spherical samples, $|\gamma_{\text{eff}}|/2\pi$ is equal to f/H_{FMR}.[16] For electron based atomic moment systems, γ_{eff} is negative. For spin only moments with a Landé g factor of 2, $|\gamma_{\text{eff}}|/2\pi$ is equal to 2.8 GHz/kOe. The linewidth ΔH_{FMR} is taken as the full width at half maximum of the profiles in (b). The ΔH_{eff} results are considered in the next section.

The table shows that the FMR fields for the TT2-111 and the 100 vol % are close to 3.2 kOe and the corresponding $|\gamma_{\text{eff}}|/2\pi$ values of about 3 GHz/kOe are slightly higher than the free electron value. These samples also show relatively narrow linewidths in the 150–170 Oe range. These represent typical FMR parameters for dense ferrite materials. This situation is not maintained for the samples with lower ferrite loadings. Here one finds higher FMR fields and much lower $|\gamma_{\text{eff}}|/2\pi$ values than one would expect for any reasonable ferrite. At the same time, one sees large departures from a Lorentzian line shape and very large increases in the linewidths by a factor of 10 or so. Such a behavior indicates irregularly shaped ferrite inclusions along with complicated interparticle dipolar interaction.

It is evident that a simple change in the ferrite loading has a drastic effect on the FMR response for these composite materials. The data show that any reduction in the ferrite loading below the 100 vol % level serves to degrade the FMR response rather severely. It is worthwhile to consider two possibilities, among many, for this degradation. First, it is likely that the imbedding process yields ferrite particles with irregular shapes, large strains, and impurities. All of these factors are known to produce large linewidths. Second, in the extreme view, one can consider the composite as a polycrystalline ferrite with a very large porosity. It is well known that even a small amount of porosity in a ferrite material can produce a large inhomogeneously broadened line. Typical porosity broadened half power linewidths for spinel ferrites at 10 GHz are in the 30–40 Oe per percent.

It may also be noteworthy that for the $L=16$ vol % sample, the FMR absorption profile is also highly distorted. The indication here is that for dilute loadings, the factors enumerated above result in more than a simple line broadening. Details of the origins of these distortions are not yet clear.

V. HIGH FIELD EFFECTIVE LINEWIDTH

The FMR results presented in the previous section show that any amount of ferroelectric loading causes a severe degradation of the linewidth. This section considers the microwave loss as measured at high field rather than at ferromagnetic resonance. In conventional ferrites, one can use high field measurements of the so-called effective linewidth to determine near intrinsic losses even when the FMR linewidth is broadened by microstructure effects or inhomogeneities of various types.[17] This section presents the results of similar measurements on the present ferrite-ferroelectric composite materials.

The high field microwave response was evaluated for the composites for a field range of 5–11 kOe at 10 GHz, and high field effective linewidth determinations were made from these data. Reasonable results were obtained for the samples with 6, 16, 27, and 100 vol % loadings. For the samples with lower L values, the high field losses were too large to obtain meaningful determinations of the effective linewidth. Section V A introduces the working equations for the high field microwave response and the effective linewidth analysis, and provides brief experimental details for the composite materials measurements. Section V B gives the experimental results.

A. Experimental procedure and data analysis

The effective linewidth technique is based on measurements of the change in the frequency f and quality factor Q with field for a high Q cylindrical microwave cavity with the magnetic sample in place. Typically, the measurement is made with applied fields well above the FMR field. For such high fields, the spin wave band is shifted well above the nominal cavity and signal frequency. This eliminates, in principle, any contribution to the magnetic losses due to any inhomogeneities that may be present in the sample.

Such measurements allow one to access the high field tail of the FMR response and determine the relaxation rate η for the driven mode that is applicable in the high field regime. Expressed in linewidth units, one can write an effective linewidth parameter $\Delta H_{\text{eff}}=2\eta/|\gamma|$. This ΔH_{eff} simply expresses the relaxation rate in field units for convenient comparison with actual linewidth data. For simplicity, the conversion from a relaxation rate to ΔH_{eff} uses the free electron gyromagnetic ratio γ rather than the γ_{eff} introduced in Sec. IV. The difference is small. In the high field regime of loss, the intrinsic γ is also more applicable.

For a typical polycrystalline ferrite, one may have a 10 GHz FMR linewidth in the 100–200 Oe range, while the high field effective linewidth will be in the 10–20 Oe range. In the case of very dense ferrites, one finds that ΔH_{eff} approaches intrinsic single crystal linewidth values in the limit of very high fields. As the results below will show, the effective linewidth situation for ferrite-ferroelectric composite materials is more complicated.

Reference 18 provides a full description of the high field effective linewidth analysis procedure for materials in which one finds a constant ΔH_{eff} in the high field regime.[18] This is the applicable situation here. The sample is placed in the center of a TE_{011} cavity with a high Q, typically in the 20 000 range. The cavity frequency f and quality factor Q are then measured as a function of the field H in the high field regime, and the data are analyzed to obtain a high field ΔH_{eff} parameter. The analysis procedure is summarized below. Details of the measurement procedure as it applies to the present composite samples are given at the end of the section.

The working cavity response equations may be written as

$$f = f_{\infty} - KX_F(H,f) \tag{1}$$

and

$$\frac{1}{Q} = \frac{1}{Q_{\infty}} + K\Delta H_{\text{eff}} X_Q(H,f). \tag{2}$$

In the above, f_∞ and Q_∞ denote the cavity frequency and quality factor, respectively, in the limit of very high fields. In this limit, the magnetic response is essentially frozen out. The K parameter takes the form

$$K = C\frac{V_m}{V_{\text{cav}}}, \tag{3}$$

where V_m denotes the active magnetic volume of the sample, C is a fixed parameter that depends on the cavity dimensions and cavity mode, and V_{cav} is the cavity volume. For the cavity used for this work, C/V_{cav} is equal to 0.109 cm^{-3}.

The $X_F(H,f)$ and $X_Q(H,f)$ denote field and frequency dependent dispersion and absorption parameters, respectively. In the case of an isotropic spherical magnetic sample, these parameters may be written as

$$X_F(H,f) = \frac{4\pi M_S H f}{H^2 - (f/|\gamma|)^2} \tag{4}$$

and

$$X_Q(H,f) = \frac{4\pi M_S[H^2 + (f/|\gamma|)^2]}{[H^2 - (f/|\gamma|)^2]^2}, \tag{5}$$

where $4\pi M_S$ is the saturation magnetic induction value for the magnetic sample. For composites, it is a reasonable choice to set $4\pi M_S$ equal to $\langle 4\pi M\rangle_{\text{sat-100}}$, since it is the uniform mode microwave response of the ferrite phase that defines the response equations listed above. Note that in the high field limit in which $H^2 \gg (f/|\gamma|)^2$ is satisfied, typically for fields above 5–6 kOe or so, the $X_F(H,f)$ scales essentially as $1/H$ and $X_Q(H,f)$ scales as $1/H^2$. The plots to be considered shortly for f vs $X_F(H,f)$ and $1/Q$ vs $X_Q(H,f)$ should be considered in this light.

From Eq. (1), one can see that the slope of the line obtained from a plot of the measured cavity frequency as a function of $X_F(H,f)$ will correspond to $-K$. From Eq. (2), one can also see that the slope of the plot of $1/Q$ as a function of $X_Q(H,f)$ will correspond to $K\Delta H_{\text{eff}}$. The ratio of the two slopes will then yield the high field effective linewidth ΔH_{eff}.

The data to be presented in the next section confirm that such linear f vs $X_F(H,f)$ and $1/Q$ vs $X_Q(H,f)$ responses are obtained for the series of composite samples of interest here. For ferrite-ferroelectric composites, however, it is also important to consider the way in which the K parameter scales with the sample mass and ferrite loading L. For the current samples, one may write the active magnetic volume as $V_m = V_s L/100$, where V_s is the density of the ferrite component. Based on this relation, one obtains a K parameter to sample volume ratio as

$$\frac{K}{V_s} = 0.001\,09L. \tag{6}$$

This simple connection provides a simple test of the effect of loading on the cavity frequency response. The volume to the measured samples ranged from 0.0722 to 0.2486 cm^3.

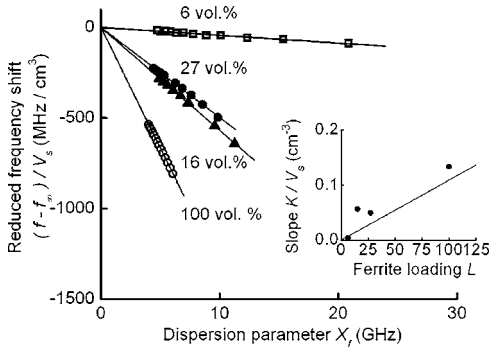

FIG. 6. Reduced cavity frequency shift $(f-f_\infty)/V_s$ as a function of the dispersion parameter X_F for the different ferrite loadings, as indicated. The solid lines show linear fits to the different data sets. The inset shows the response slope parameter K/V_s as a function of the ferrite loading L. The solid circles in the inset show the slopes of line fits in the main graph, and the line shows the calculated theoretical response based on microwave perturbation theory.

B. High field effective linewidth results

Figure 6 shows measurement results for the cavity frequency shift as a function of field. The data in the main graph are shown in an $(f-f_\infty)/V_s$ vs X_F format for the 6, 16, 27, and 100 vol % samples, as indicated. The solid lines show linear fits to the different data sets. The solid points in the inset show the slopes of line fits as a function of the loading L for the different samples, and the straight line shows the expected slope response from Eq. (6).

The X_F values were obtained from the raw f vs H data and Eq. (4). The $(f-f_\infty)/V_s$ format for the vertical axis display was used so that all the data for the samples with different loadings could be compared in a consistent manner. While the extrapolated f_∞ values vary from sample to sample, depending on the overall cavity loading, a display based on $(f-f_\infty)/V_s$ will extrapolate to a vertical axis value of zero in the $X_F=0$ limit. From Eq. (6), one sees that the K parameter scales with the sample volume V_s. The slope of a given $(f-f_\infty)/V_s$ vs X_F plot, therefore, should scale with the loading L.

All of the data plots in Fig. 6 confirm the expectation from Eq. (1) that $(f-f_\infty)/V_s$ is a linear function of X_F with a negative slope. The general trend of the slopes from these plots to scale with the loading L, with the notable exception of $L=16$ vol %, is also consistent with the expectation from Eqs. (1) and (6). The slope results in the inset make this trend quantitative and show that the response is reasonably close (except for the $L=16$ vol % point) to the solid line result from perturbation theory. The fact that the fitted slope values from the data fall about 10 vol % above the solid line is consistent with sample loading effects measured by Truedson *et al.*[18]

It is not clear why the $(f-f_\infty)/V_s$ vs X_F response for the 16 vol % sample should be so anomalous. There is no inconsistency in the corresponding static magnetization versus field date that would point to such a large anomaly in the off-resonance microwave response.

Figure 7 shows corresponding results on the inverse cavity Q factor as a function of field. The data in the main graph are shown in a $(1/Q-1/Q_\infty)/K$ vs X_Q format for the same

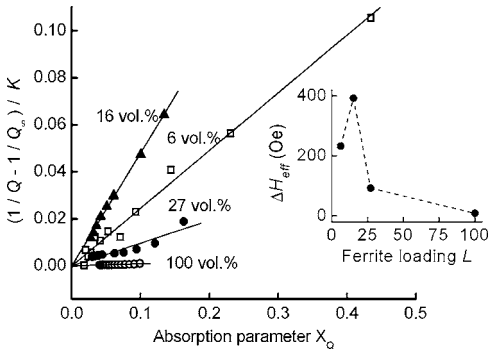

FIG. 7. Reduced sample loss parameter $(1/Q-1/Q_\infty)/K$ as a function of the absorption parameter X_Q, for the different loadings of the ferrite, as indicated. The inset shows the calculated effective linewidth ΔH_{eff} as a function of ferrite loading L.

samples as those used for the data in Fig. 6. The format is the same as for Fig. 6. The solid lines show linear fits to the different data sets. The solid points in the inset shows the slopes of line fits as a function of the loading L for the different samples.

The X_Q values were obtained from the raw f vs H data and Eq. (5). The $(1/Q-1/Q_\infty)/K$ format for the vertical axis display was used so that the data for the samples with different loadings could be compared in a consistent manner. For a linear $(1/Q-1/Q_\infty)/K$ vs X_Q response, moreover, one can see from Eq. (2) that the slope for a given data set corresponds directly to the high field effective linewidth ΔH_{eff}.

All of the data plots in Fig. 7 confirm the expectation from Eq. (2) that $(1/Q-1/Q_\infty)/K$ is a linear function of X_Q with a positive slope. This means, as noted above, that one has a well defined high field effective linewidth that corresponds to the slope of the response for each data set. As the inset to Fig. 7 shows, with the exception of the data for $L=16$ vol %, there is a general trend in these slopes, and hence ΔH_{eff}, to decrease as the loading is increased. The actual fits give relatively small effective linewidth values of 8 Oe at $L=100$ vol %, 93 Oe at $L=27$ vol %, and 392 Oe at $L=16$ vol %, and 232 Oe at $L=6$ vol %. As a point of reference, the TT2-111 material had $\Delta H_{\text{eff}}=6$ Oe. It is important to note that the anomalously large slope and corresponding ΔH_{eff} value of 392 Oe for the $L=16$ vol % sample is not a carryover from the anomaly noted for the $(f-f_\infty)/V_s$ vs X_F response discussed above. This anomaly is normalized out by the K divisor in the vertical axis display used for Fig. 7. This anomalously large ΔH_{eff} provides evidence in its own right that there is something problematic about this sample. These ΔH_{eff} values are the same as those listed in Table I.

There are several effects that are passed over in the $(1/Q-1/Q_\infty)/K$ vs X_Q display format used for Fig. 7. This relates to the actual values of the high field Q that lead to the $1/Q_\infty$ offset in the first place. It was found that a decrease in loading to the 16 or 6 vol % level caused a significant drop in the Q_∞ values for the cavity. Typical Q_∞ values for the cavity with the TT2-111 sample, the 100 vol % composite, were in the 20 000–22 000 range. It is interesting to note that even a drop in loading to 27 vol % caused only a drop in Q_∞ value to about 20 000. These values amount to a very small degradation from the nominal empty cavity Q of 22 500 or so. For the 16 and 6 vol % loading samples, however, the Q_∞ is degraded to about 7000 and 5000, respectively.

The fact that the K/V_s value for the $L=6$ vol % sample, as shown in the Fig. 6 inset, is consistent with the corresponding values for the 27 and 100 vol % samples indicates that the drop in Q did not affect the cavity calibration. It is possible, however, that the factor of 4 ΔH_{eff} increase in going from $L=27$ vol % to $L=6$ vol % could be due to the same process that causes the factor of 4 drop in Q_∞. It is possible that the large ferroelectric component introduces Ohmic losses that affect both Q_∞ and ΔH_{eff}. Truedson *et al.*[18] have shown that Ohmic losses in a ferrite disk can give the appearance of a contribution to the high field ΔH_{eff}.

VI. DIELECTRIC PROPERTIES

Three specific dielectric properties as a function of loading were measured: the dielectric constant, the loss tangent $(\tan\delta)$, and the electric field tunability. Measurements of the dielectric constant and dielectric loss tangent were made at 1 MHz and 10 GHz. The 1 MHz measurements were made with a Hewlett Packard (HP) impedance gain/phase analyzer.[19] The 10 GHz measurements were obtained with a 10 GHz cavity resonator and a HP vector network analyzer. The tunability determinations were based on measurements at 1 MHz of a change in capacitance with applied voltage for the electroded disk samples discussed in Sec. II. For the present purposes, the tunability is taken as $T=\delta C/C$, where C is the nominal capacitance at zero voltage and δC is the measured change.

Table II and Figs. 8–10 summarize the results of the dielectric property measurements. The table gives numerical values on the relative dielectric constant ε_r, the loss tangent $\tan\delta$, and the electric field tunability T. The ε_r and $\tan\delta$ are taken at 1 MHz and 10 GHz, while the tunability values are taken at two values of the electric fields, 2 and 4 V/μm. In general, one can see that the dielectric constant ε_r and tunability T tend to decrease as the ferrite loading is increased, but the change does not scale linearly with loading. The composite loss tangent data show low values at 1 MHz and

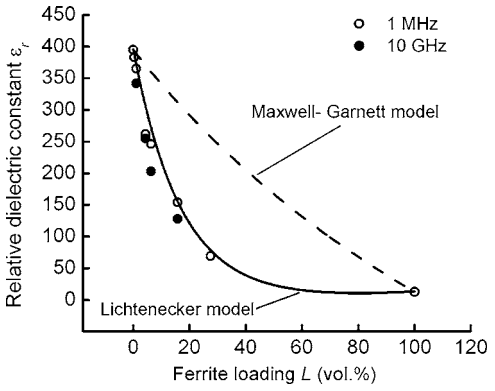

FIG. 8. Relative dielectric constant ε_r as a function of the ferrite loading L. The solid circles show the 10 GHz data. The open circles show the 1 MHz data. The dashed curve is a calculation based on the Maxwell-Garnett model and the solid curve is a calculation based on the Lichtenecker model for inclusions in a dielectric matrix.

TABLE II. Summary of dielectric property measurements.

Vol. % ferrite loading L	Relative dielectric constant at 1 MHz	Relative dielectric constant at 10 GHz	Dielectric loss tangent (tan δ) at 1 MHz	Dielectric loss tangent (tan δ) at 10 GHz	Tunability (%)	
					2 V/μm	4 V/μm
100	12.6	⋯	0.0390	⋯	⋯	⋯
27	69	⋯	0.0069	⋯	3.2%	6.8%
16	154	128	0.0025	0.0301	8.5%	16.0%
6	246	203	0.0019	0.0279	9.0%	19.0%
4	262	255	0.0018	0.0245	8.0%	19.0%
1	365	342	0.0009	0.0191	11.0%	24.0%
0.3	383	⋯	0.0006	⋯	12.0%	25.0%
0	395	412	0.0010	0.0235	17.0%	29.0%

high values at 10 GHz that then switch from low to high (1 MHz) and high to low (10 GHz) for the pure ferrite.

Figure 8 shows results for the relative dielectric constant ε_r as a function of ferrite loading. The open and solid circles show the data for 1 MHz and 10 GHz, respectively. The solid and dashed curves show computed ε_r vs L responses based on two commonly used dielectric response models for mixtures.[20] The solid curve is for the Lichtenecker model and the dashed curve is for the Maxwell-Garnett model.

There is a very rapid initial decrease in ε_r with L at the lower loading values and an apparent leveling off in the $L=50-60$ vol % range. It is clear from the theoretical curves that the Lichtenecker model fits the data nicely. This model is essentially a power law rule for inclusions in a dielectric matrix. Such a rule appears to account nicely for the initial rapid drop in ε_r with L. It is clear that the Maxwell-Garnett model based on spherical inclusions in a dielectric matrix does not fit the data.

Figure 9 shows results on tan δ as a function of ferrite loading at 1 MHz and 10 GHz, as indicated. Data were obtained for L values up to 27 vol %. The inset shows the 1 MHz data for L values up to 6 vol % on an expanded scale. These data show a slow and gradual increase in tan δ with L. The 10 GHz values are much larger, increase more rapidly, and show a bigger spread than the 1 MHz data. The results for 10 GHz are somewhat perplexing. Catalog values of tan δ for commercial TT2-111 at 10 GHz are in the 0.0001 range.

Figure 10 shows results for the normalized tunability parameter T as a function of L. The open and solid circles show the data for electric field values of 2 and 4 V/μm, respectively. The data sets for the two fields appear to track each other and show that the electric tunability decreases, as the ferrite loading is increased. Except for the initial dip in T at low L, the trend of the response is nearly linear.

Overall, one can say that the effect of the ferrite loading on ε_r is consistent with well established mixing models and that the loading reduces the electric tunability of the composite. The ferrite loading has an adverse effect on the dielectric loss, especially at microwave frequencies. The large tan δ values at 10 GHz represent a significant challenge. It is clear that significant advances in preparation methods will be needed in order to produce low dielectric loss composite materials for microwave applications.

VII. SUMMARY

The above sections have described preparation methods and measurement results on the magnetic and dielectric properties a ferrite-ferroelectric composite fabricated from a Paratek barium strontium titanate material and a Trans-Tech nickel zinc ferrite TT2-111 material. The ferrite loading levels were varied from the pure BSTO material ($L=0$) to pure TT2-111 ($L=100$ vol %). Initial susceptibility, saturation field, and coercive force data show trends consistent with the saturation induction results.

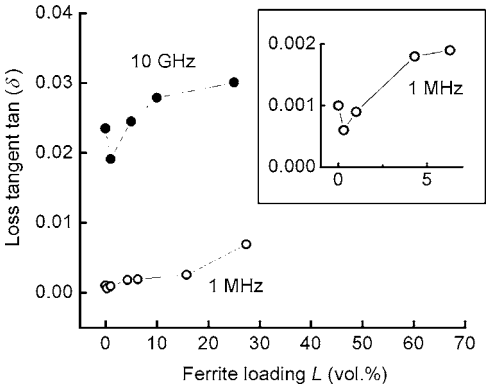

FIG. 9. Loss tangent tan δ as a function of ferrite loading L. The solid circles are the data at 10 GHz, whereas the open circles are the data at 1 MHz. The inset shows the low L 1 MHz data on an expanded scale.

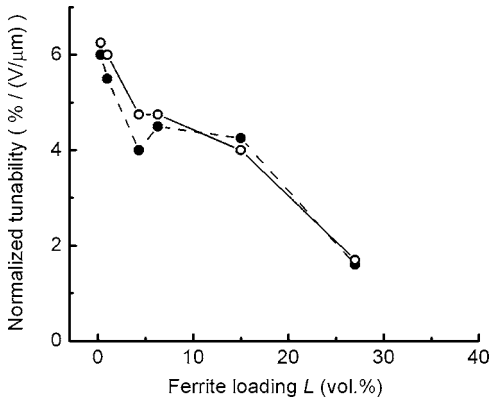

FIG. 10. Normalized tunability T as a function of ferrite loading L. The open and solid circles show the data for electric field values of 2 and 4 V/μm, respectively.

The magnetic and electric responses at high frequency show similar effects. Any amount of BSTO added to the ferrite phase causes a severe degradation in the FMR profile and linewidth as well as the high field off-resonance effective linewidth. Similarly, any amount of ferrite added to the BSTO causes a rapid drop in the relative dielectric constant and electrical tunability. The tan δ data indicate modest values in the 0.001–0.005 range at 1 MHz but much larger values in the 0.02–0.03 range at 10 GHz.

The XRD data and a comparison of magnetic properties for the $L=100$ vol % material and a commercial TT2-111 base line sample indicate that the processing recipe used for the composite materials did not cause any degradation in the NZF or the BSTO phase. The actual composites, on the other hand, all show a clear degradation in both the magnetic and the electric properties.

The static magnetic and dielectric constant results point to a model of unmodified spherical NZF inclusions in a nonmagnetic matrix. The FMR and high field effective linewidth results show that the presence of interactions between the two phases, the shape of the NZF inclusions, and extreme dilution due to the large amount of ferroelectric material can affect the magnetic losses. The addition of even a small amount of the NZF phase causes a degradation in the dielectric loss. Further work is needed to develop fabrication processes that can preserve the desirable ferroelectric and ferrite properties of the composite while, at the same time, producing a multifunctional material with enhancements in both classes of properties.

ACKNOWLEDGMENTS

This work was initiated under a U.S. Army Research Office (USARO) short-term innovative research program, Grant No. DAAD19-99-1-0170, and followed to completion under U.S. Army Research Office, MURI Grant No. W911NF-04-1-0247, USARO-DARPA (Defense Advanced Research Projects Agency) Grant No. W911NF-06-1-0163, and Office of Naval Research (U.S.) Grant No. N00014-06-1-0889. The participants are indebted to Elwood Hoakenson and Trans-Tech, Inc., Adamstown, Maryland for a sample of TT2-111 ferrite for static and microwave magnetic characterizations. Dr. William Wilber of CelWave Corporation, Marlboro, New Jersey, Dr. James Baker-Jarvis and Dr. Pavel Kabos of the National Institute of Standards and Technology, Boulder, Colorado, and Professor Gopalan Srinivasan of Oakland University, Rochester, Michigan are acknowledged for helpful discussions on ferrite-ferroelectric composite materials. Michael Varney is acknowledged for his assistance with the static magnetic measurements. Dr. Sandeep Kohli is acknowledged for his assistance with the x-ray diffraction measurements.

[1] R. Valenzuela, *Magnetic Ceramics* (Cambridge University Press, Cambridge, 1994).
[2] L. C. Sengupta and S. Sengupta, IEEE Trans. Ultrason. Ferroelectr. Freq. Control **44**, 793 (1997).
[3] F. A. Miranda, G. Subramanyam, F. W. Van Keuls, R. R. Romanofsky, J. D. Warner, and C. H. Mueller, IEEE Trans. Microwave Theory Tech. **48**, 1181 (2000).
[4] X. Qi, J. Zhou, Z. Yue, Z. Gui, and L. Li, J. Magn. Magn. Mater. **269**, 352 (2004).
[5] D. J. Bergman, Phys. Rep., Phys. Lett. **43**, 377 (1978).
[6] D. J. Bergman, Phys. Rev. B **19**, 2359 (1979).
[7] D. J. Bergman, Phys. Rev. B **23**, 3058 (1981).
[8] D. J. Bergman and D. Stroud, Solid State Phys. **46**, 147 (1992).
[9] D. J. Bergman, O. Levy, and D. Stroud, Phys. Rev. B **49**, 129 (1994).
[10] D. M. Grannan, J. C. Garland, and D. B. Tanner, Phys. Rev. Lett. **46**, 375 (1981).
[11] D. E. Aspnes, Phys. Rev. Lett. **48**, 1629 (1982).
[12] C. A. Grimes and D. M. Grimes, J. Appl. Phys. **69**, 6168 (1991).
[13] B. Abeles, H. L. Pinch, and J. I. Gittleman, Phys. Rev. Lett. **35**, 247 (1975).
[14] T. Kanai, S. Ohkoshi, A. Nakajima, T. Watanabe, and K. Hashimoto, Adv. Mater. (Weinheim, Ger.) **13**, 487 (2001).
[15] J. V. Mantese, A. L. Micheli, D. F. Dungan, R. G. Geyer, J. Baker-Jarvis, and J. Grosvenor, J. Appl. Phys. **79**, 1655 (1996).
[16] M. Sparks, *Ferromagnetic Relaxation Theory* (McGraw-Hill, New York, 1964).
[17] C. E. Patton, in *Magnetic Oxides*, edited by D. J. Craik (Wiley, London, 1975), pp. 575–645.
[18] J. R. Truedson, P. Kabos, K. D. McKinstry, and C. E. Patton, J. Appl. Phys. **76**, 432 (1994).
[19] R. G. Geyer, J. Krupka, L. Sengupta, and S. Sengupta, Proceedings of the Tenth IEEE International Symposium on Applications of Ferroelectrics, 1996 (unpublished), Catalog No. 96CH35948, p. 851.
[20] A. Sivhola, *Electromagnetic Mixing Formulas and Applications* (The Institution of Engineers, London, UK, 1999).